**Electronic Supplementary Information**

# Gate-tunable diode and photovoltaic effect in an organic-2D layered material p-n junction

Saül Vélez[a,†], David Ciudad[a,†], Joshua Island[b], Michele Buscema[b], Oihana Txoperena[a], Subir Parui[a], Gary A. Steele[b], Fèlix Casanova[a,c], Herre S. J. van der Zant[b], Andres Castellanos-Gomez[b,d,*], Luis E. Hueso[a,c,*]

[a] CIC nanoGUNE, 20018 Donostia-San Sebastian, Basque Country, Spain

[b] Kavli Institute of Nanoscience, Delft University of Technology, Lorentzweg 1, 2628 CJ Delft, The Netherlands

[c] IKERBASQUE, Basque Foundation for Science, 48011 Bilbao, Basque Country, Spain

[d] Instituto Madrileño de Estudios Avanzados en Nanociencia (IMDEA-Nanociencia), 28049 Madrid, Spain

[†] These authors have contributed equally to this work

* E-mail: (A.C.-G.) andres.castellanos@imdea.org, (L.E.H.) l.hueso@nanogune.eu

### S1. $I_{ds}$-$V_{ds}$ curves of the $MoS_2$ and the CuPc field effect transistors (FETs)

In our CuPc-$MoS_2$ devices, two metal electrodes were defined on the $MoS_2$ flake. The FET characteristics of the $MoS_2$ layer can be measured using these two electrodes as drain and source contacts, and a third contact on the $Si^{++}$ substrate as the gate (Fig. S1a shows a sketch of the electrical connections). CuPc FETs were also fabricated in the same wafer to characterize the electrical properties of the organic film. We used Ti (work function 4.3 eV) to contact the $MoS_2$ flake (electron affinity 4.2 eV) in order to prevent the formation of a large Schottky barrier. For the same reason, we used Au to contact the CuPc (Au work function is 5.3 eV and the HOMO level of the CuPc is at 5.2 eV). Fig. S1b and S1c show the $I_{ds}$-$V_{ds}$ characteristics measured at different $V_g$ values for two representative $MoS_2$ and CuPc FETs, respectively. Insets of Fig. S1b and S1c show a zoom of the $I_{ds}$-$V_{ds}$ curves in the small bias regime. The first linear trend is indicative of quasi-ohmic contact achieved in the metal-semiconductor junctions. A deviation from the linearity is observed at large $V_{ds}$ values in both cases (note that this is only achievable in truly metallic contacts).

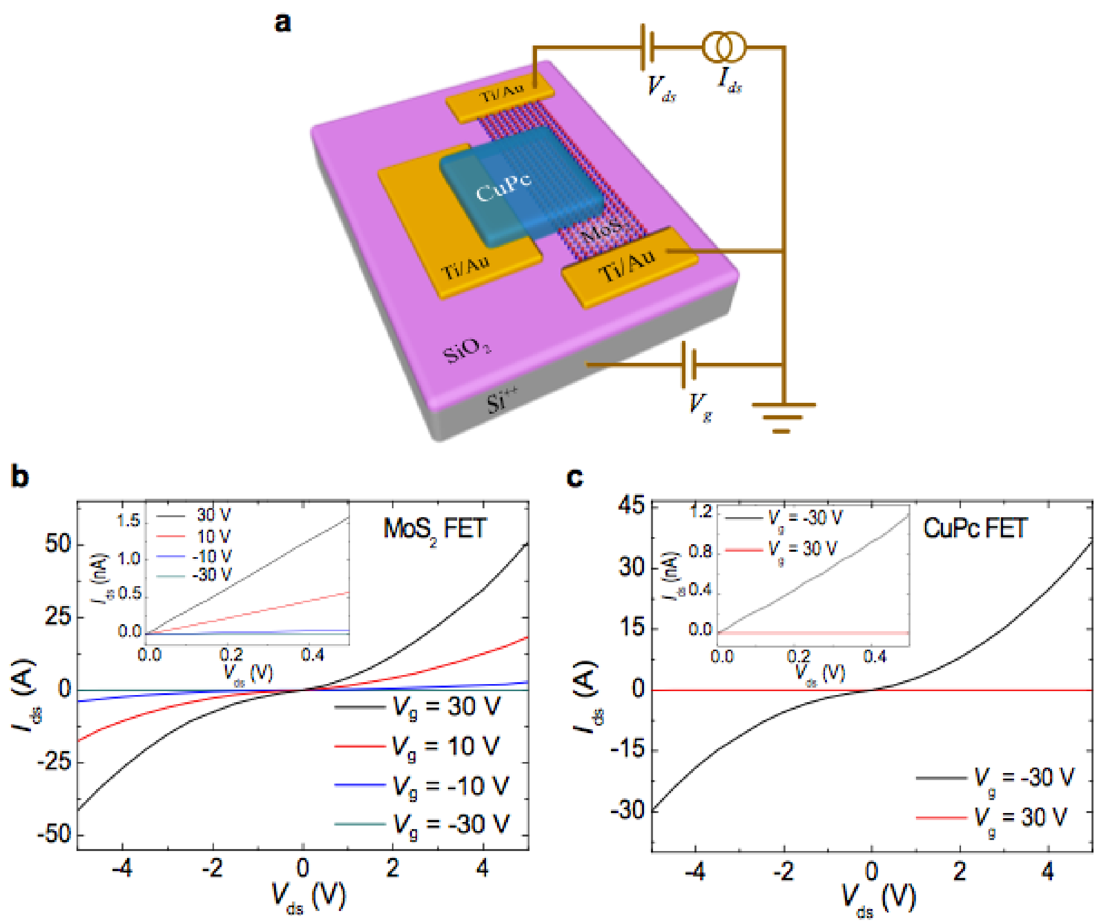


**Fig. S1** Characterization of the metal-semiconductor contacts. (a) Schematics of the contacts made in our CuPc-$MoS_2$ devices to characterize the FET characteristics of the $MoS_2$ flakes (contacts for a CuPc FET are not shown here). (b) and (c) $I_{ds}$-$V_{ds}$ curves of a representative $MoS_2$ and CuPc FETs, respectively, measured at different gate voltages. Insets in (b) and (c) show a zoom in the first quadrant of the $I_{ds}$-$V_{ds}$ curves. The quasi-linear behavior at small bias values indicates small Schottky barrier formation (quasi-ohmic contacts) at the metal-semiconductor contacts. A deviation from the linearity is observed at large $V_{ds}$ values.

## S2. Conduction of the CuPc-$MoS_2$ heterojunction

As a first approximation, the total resistance of the CuPc-$MoS_2$ heterostructure can be modeled as two resistances in series: one resistance due to the CuPc film and the other related to the $MoS_2$ flake, giving $R_H = R_{CuPc} + R_{MoS2}$. In our devices, we can measure/estimate the resistances of the CuPc and the $MoS_2$ by individually characterizing both the CuPc and the $MoS_2$ FETs, in addition to the CuPc-$MoS_2$ FET. We denote $R_H = V_H/I_H$ as the resistance of the CuPc-$MoS_2$ FET heterojunction; $R_{CuPc} = V_{CuPc}/I_{CuPc}$ for the CuPc FET; and $R_{MoS2} = V_{MoS2}/I_{MoS2}$ for the $MoS_2$ FET. If we fix the voltage of all devices to the same $V_{ds}$, the current passing through the heterojunction is given by $I_H = V_H/(R_{MoS2}+R_{CuPc})$. Using the relations given above one gets

$$I_H = (I_{CuPc} \cdot I_{MoS2})/(I_{CuPc}+I_{MoS2}). \tag{S1}$$

Notice that $I_{CuPc}$ and $I_{MoS2}$ are not the currents passing through the layers of the heterostructure when applying a voltage $V_{ds}$, but the currents measured in each individual FET when applying a voltage $V_{ds}$. This relation allows us to reproduce the experimental data $I_{ds}(V_g)$ obtained for a CuPc-$MoS_2$ FET (for instance, the red curve in Fig. 2a) from the measured individual FETs (see blue and black curves in Fig. 2a). Fig. S2 shows the transfer curves of both CuPc and $MoS_2$ FETs extracted from Fig. 2a together with the calculated transfer curve for the heterojunction using Equation S1 (note that the FET characteristics of the $MoS_2$ flake was scaled to account for the different $V_{ds}$ used). There is a good qualitative agreement between the experimental data and the calculated transfer curve (red straight line in Fig. 2a vs red squares plotted in Fig. S2). Notice that the exact solution (which is out of our scope here) might also account for other factors as for differences in the geometry for the conducting channels, screening effects in the CuPc layer when measuring the CuPc-$MoS_2$ devices, etc.

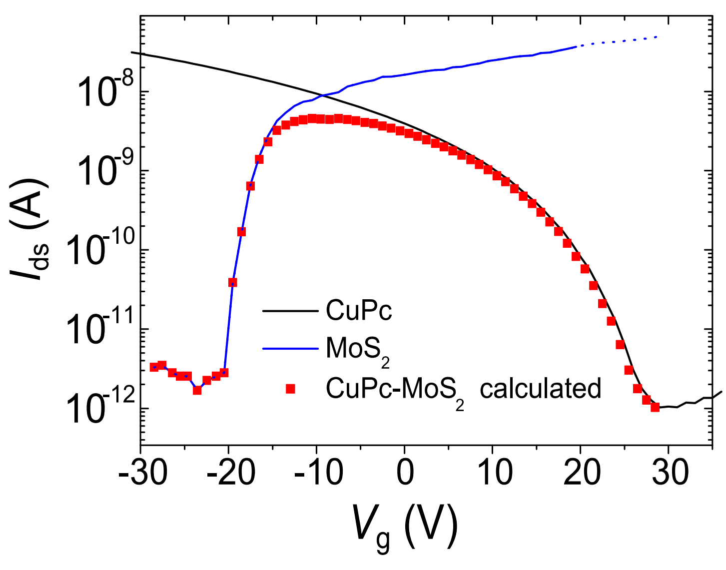


**Fig. S2** Calculated transfer curve of the CuPc-$MoS_2$ FET (red) from the experimental curves of the individual FETs ($MoS_2$-blue and CuPc-black) using Equation (S1). Original data extracted from Fig. 2a.

**S3. Electrical characterization of one of the monolayer-$MoS_2$-based CuPc-$MoS_2$ device**

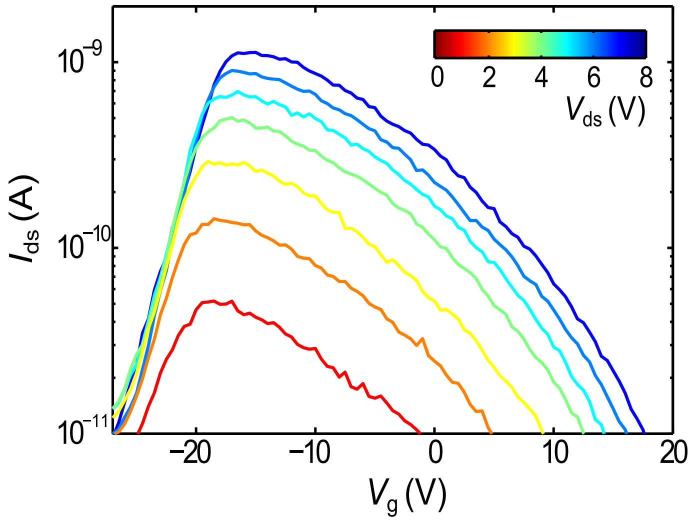


**Fig. S3** Transfer curve $I_{ds}$-$V_g$ of a representative CuPc-$MoS_2$ FET made of a monolayer $MoS_2$. These curves resemble the ones obtained with a bilayer-based CuPc-$MoS_2$ device (Fig. 2b). Similar results were obtained among different CuPc-$MoS_2$ p-n junction devices (for both monolayer- and bilayer-$MoS_2$-based devices).

## S4. Fits of the diode characteristics to the Shockley equation

In this section, we model the $I_{ds}$-$V_{ds}$ characteristics of the p-n junction for a representative CuPc-$MoS_2$ device with a modified form of the Shockley equation. In an ideal case, the relationship between the current $I_{ds}$ and the voltage bias $V_{ds}$ across a p-n diode is described by the Shockley model:

$$I_{ds} = I_s\left[\exp\left(\frac{V_{ds}}{nV_T}\right) - 1\right], \tag{S2}$$

where $I_s$ is the saturation current, $n$ is the ideality factor, $V_T = k_B T$ ($k_B$ is the Boltzmann constant in eV/K and $T$ is the temperature in K) is the thermal voltage. The ideality factor is related to the carrier recombination mechanisms at the p-n junction; $n = 1$ indicates that there is only band-to-band recombination of minority carriers, which is the ideal case.

A more realistic model should include current losses due to parasitic resistances in parallel ($R_{p,}$ also called *shunt resistance*) and in series ($R_S$) with the junction. A schematic of the model circuit is presented in the inset of Fig. S4a. The series resistance $R_S$ models the voltage losses due to e.g. contact resistance or the resistance associated to long leads of high resistivity. The parallel resistance $R_p$ models additional carrier recombination mechanisms that drain current from the junction. The slope of the measured $I_{ds}$-$V_{ds}$ curves at $V_{ds}$ = 0 V indicates a non-infinite $R_p$. To include these effects, we can rewrite Equation (S2) as

$$I_{ds} = I_s\left[\exp\left(\frac{V_{ds} - I_{ds}R_s}{nV_T}\right) - 1\right] + \frac{V_{ds} - I_{ds}R_s}{R_p}. \tag{S3}$$

An analytical expression can be obtained in the following form [S1]

$$I_{ds} = \frac{nV_T}{R_s} W\left[\frac{I_s R_s R_p}{nV_T(R_s + R_p)} \exp\left(\frac{R_p(V_{ds} - I_s R_s)}{nV_T(R_s + R_p)}\right)\right] + \frac{V_{ds} - I_s R_p}{R_s + R_p}, \tag{S4}$$

where $W$ is the Lambert $W$-function.

The fits of the measured $I_{ds}$-$V_{ds}$ curves in a CuPc-$MoS_2$ (bilayer based) device to the Equation (S4) are shown in Fig. S4. We summarized the extracted model parameters in Table S1.

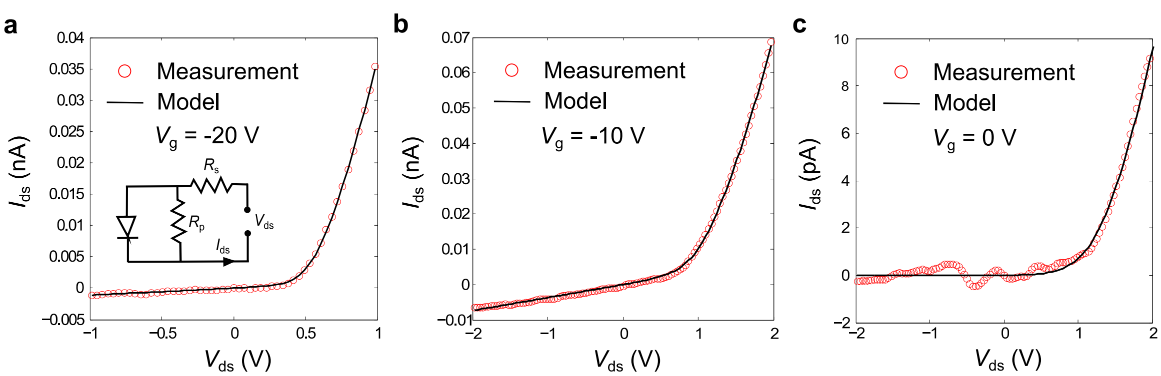

**Fig. S4** Fits of the $I_{ds}$-$V_{ds}$ diode-characteristics of the CuPc-$MoS_2$ junction to Equation (S4) for different gate voltages -20 V (a), -10 V (b) and 0 V (c). Inset of panel (a) shows the schematics of the model. Table S1 shows a summary of the extracted parameters.

| | $V_g$ = -20 V | $V_g$ = -10 V | $V_g$ = 0 V |
|---|---|---|---|
| $I_S$ (μA) | 4.23 | 1.63 | 7.65 |
| $n$ | 2.87 | 3.97 | 8.25 |
| $R_S$ (GΩ) | 9.15 | 14.39 | 50.6 |
| $R_p$ (GΩ) | 874.1 | 239.1 | >1000 |

**Table S1** Summary of the main parameters extracted from the fittings shown in Fig. S4.

## S5. Photogating of the CuPc-$MoS_2$ devices

The photoresponse of the CuPc-$MoS_2$ heterostructure (Fig. 3a) can be modeled as a shift of the transfer curve of the $MoS_2$ layer towards (more) negative $V_g$ values (n-type doping). This shift can be explained via electron doping caused by the photogenerated charges in the CuPc layer, which might be captured in long-lived trap states at the CuPc-$MoS_2$ interface itself or close to the junction. This behavior is known as photogating, and already reported to occur for $MoS_2$ [S2].

To illustrate the effect, Fig. S5a shows the transfer curve of a $MoS_2$-CuPc FET (red) calculated from the transfer curves of a CuPc (black) and a $MoS_2$ (blue) FETs (corresponding data of Fig. S2; see Supplementary Section S2 for more details) obtained in dark conditions. The n-doping of the $MoS_2$ layer under illumination can be simulated by mathematically adding an offset to the $MoS_2$ FET curve (dashed blue line in Fig. S5). Using this simulated curve and the transfer characteristics of the CuPc FET, the transfer curve of the CuPc-$MoS_2$ under illumination is also calculated and included in Fig. S5 (dashed red curve). For sake of comparison, the transfer curves of the CuPc-$MoS_2$ device in dark conditions (straight black curve) and under illumination (dashed red curve) are plotted in Fig. S5b in the linear scale. The simulated photogating effect agrees quite well with the photoresponse shown in Fig. 3a. Note that the differences between the characteristics of this device and the one shown in Fig. 3a are attributed to different doping of the constituent layers.

One could also consider that photogating in the CuPc layer might also occur (in that case, the transfer curve would be moved towards positive values), but the sharper subthreshold characteristics of the $MoS_2$ layer makes n-doping of the $MoS_2$ layer dominant over p-doping of the CuPc, if there is any.

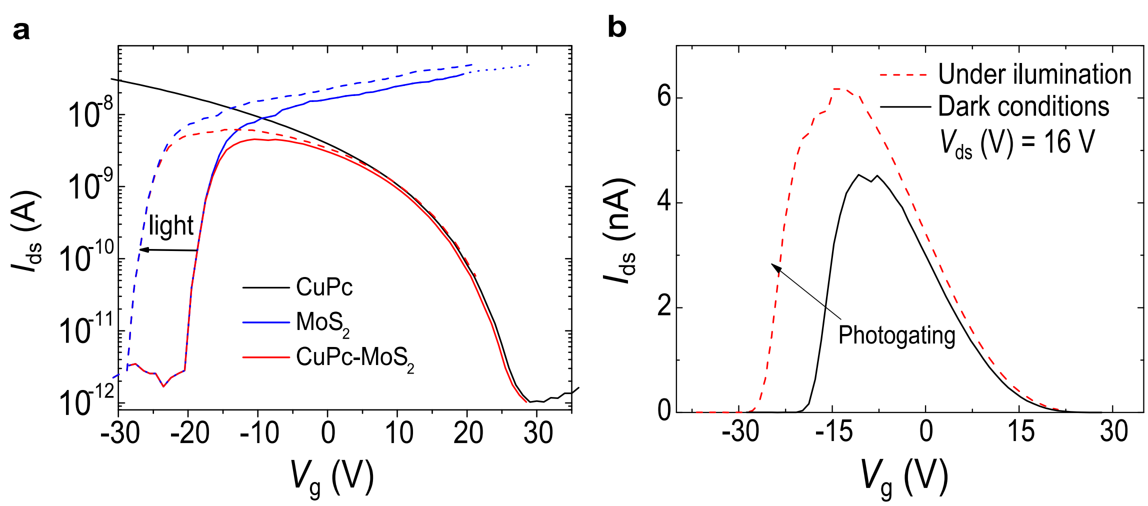


**Fig. S5** Simulated photogating of the CuPc-$MoS_2$ devices. (a) CuPc (black straight line) and $MoS_2$ (blue straight line) FETs. Data corresponding to the device explored in Fig. 2a. Calculated transfer curve for the CuPc-$MoS_2$ device (red straight line) as explained in Supplementary Section 2. The simulated photogating of the $MoS_2$ layer ($\Delta V_g$ = -8 V) is represented as a dashed blue line. Dashed red line shows the calculated CuPc-$MoS_2$ transfer curve characteristics considering the photogating effect. (b) Linear plot of the calculated CuPc-$MoS_2$ transfer curves for both dark conditions (blak straight line) and simulated under illumination (red dashed line). The curves shown here captures the behavior observed in Fig. 3a.

## S6. Gate dependence of the photoinduced current in the CuPc-$MoS_2$ p-n junction

The photoinduced current ($I_{ph}$) of the CuPc-$MoS_2$ p-n junction is calculated by subtracting the source-drain current measured in dark conditions ($I_d$) to the one measured under illumination ($I_l$ ): $I_{ph}= I_l - I_d$, at a given $V_{ds}$ and $V_g$. Fig. S6a schematically represents the generated $I_{ph}$ (indicated by a vertical dashed arrow) at a particular $V_g$ value ($V_g$ ~ -30 V) measured at $V_{ds}$ = 16 V. Fig. S6b shows a 2D colored plot of the $I_d$ measured as a function of both the $V_{ds}$ (x-axis) and $V_g$ (y-axis). By performing the same measurements under illumination $I_l(V_{ds},V_g)$, the $I_{ph}(V_{ds},V_g)$ 2D map is calculated and plotted in Fig. S6c. The main feature of the photoresponse is associated to the shift experienced in the $V_g$ value where the maximum of the $I_{ph}$ appears with respect to the $I_d$. This effect is explained via photogating (see Supplementary Section S5).

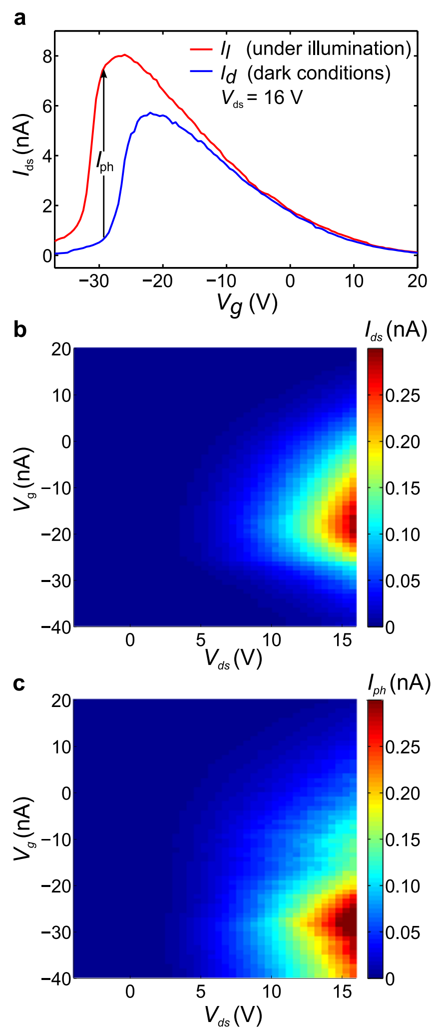


**Fig. S6** Gate dependence of the photoinduced current in the CuPc-$MoS_2$ junction. (a) $I_{ds}$-$V_g$ curves measured in dark conditions ($I_d$) and under illumination ($I_l$) at $V_{ds}$ = 16 V. (b) 2D colored map of the current measured in dark conditions $I_d$. (c) Photoinduced current $I_{ph} = I_l - I_d$ as a function of $V_{ds}$ and $V_g$. The strong shift in $V_g$ observed between dark conditions and under illumination is explained via photogating of the $MoS_2$ layer. Under illumination, a maximum increase of the $I_{ds}$ of up to two orders of magnitude is measured with respect to dark conditions.

**S7. Dataset of the optoelectronics characterization of a CuPc-$MoS_2$ monolayer-based device**

The photovoltaic effect in a monolayer-$MoS_2$-based CuPc-$MoS_2$ device has been explored as a function of the gate voltage (Fig. S7), wavelength (Fig. S8) and incident laser power (Fig. S9). Qualitatively, similar results compared to the bilayer CuPc-$MoS_2$ device (Fig. 4) are found. Quantitatively, slightly larger $V_{OC}$ voltages are obtained in this case, which might be attributed to a change in the band-gap between monolayer and bilayer $MoS_2$, resulting in a slightly different band-alignment with the CuPc film. We would like to comment here that during the characterization of the monolayer CuPc-$MoS_2$ we experienced some leakage problems, making the data measured in this case more noisy/less accurate than in the bilayer case.

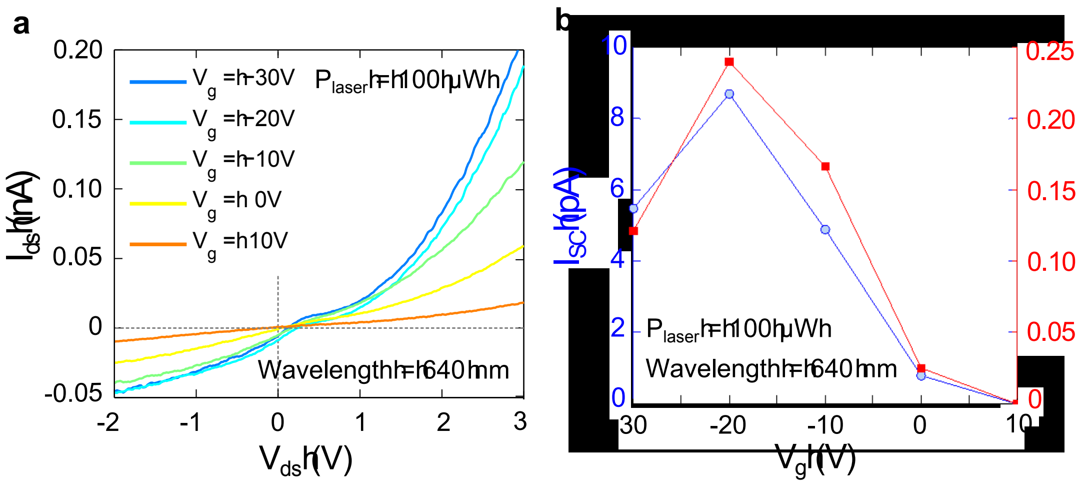


**Fig. S7** Gate dependence on the photovoltaic effect of a CuPc-$MoS_2$ monolayer-based device. (a) $I_{ds}$-$V_{ds}$ curves measured at different $V_g$ values under illumination with $P_{laser}$ = 100 mW and $\lambda$ = 640 nm. (b) $I_{SC}$ and $V_{OC}$ values extracted from (a). The maxima in the $I_{SC}$ and $V_{OC}$ values are found around the region where the diode shows better ideality factors, and correlates with the maxima of the conductivity of the p-n junction.

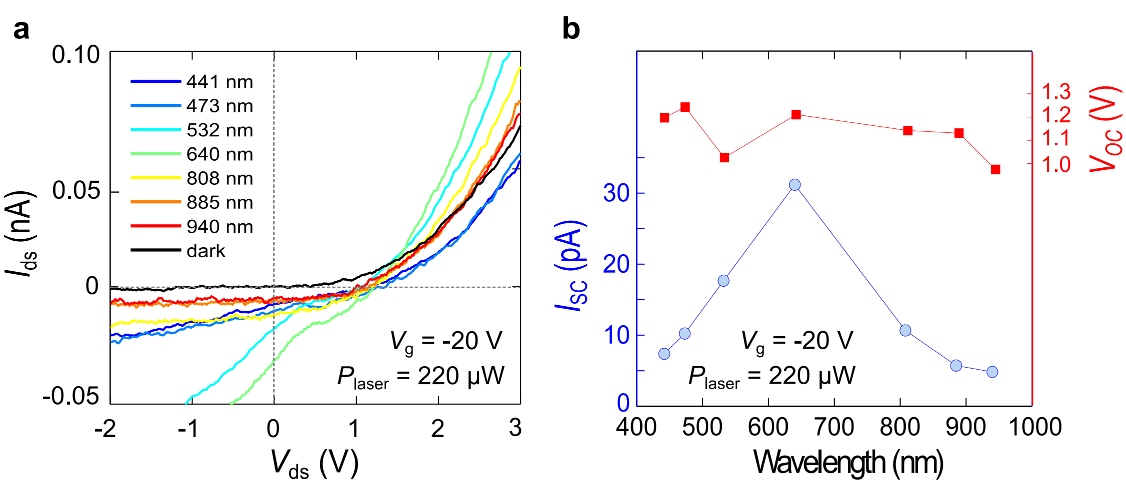


**Fig. S8** Wavelength dependence on the photovoltaic effect of a CuPc-$MoS_2$ monolayer-based device. (a) $I_{ds}$-$V_{ds}$ curves measured under illumination at different wavelengths. Measurements taken at fixed $V_g$ = -20 V and $P_{laser}$ = 220 $\mu$W. (b) $I_{SC}$ and $V_{OC}$ values extracted from (a). Fairly constant large $V_{OC}$ are obtained at all wavelengths whereas the $I_{SC}$ values follow the absorption edge of the CuPc layer.

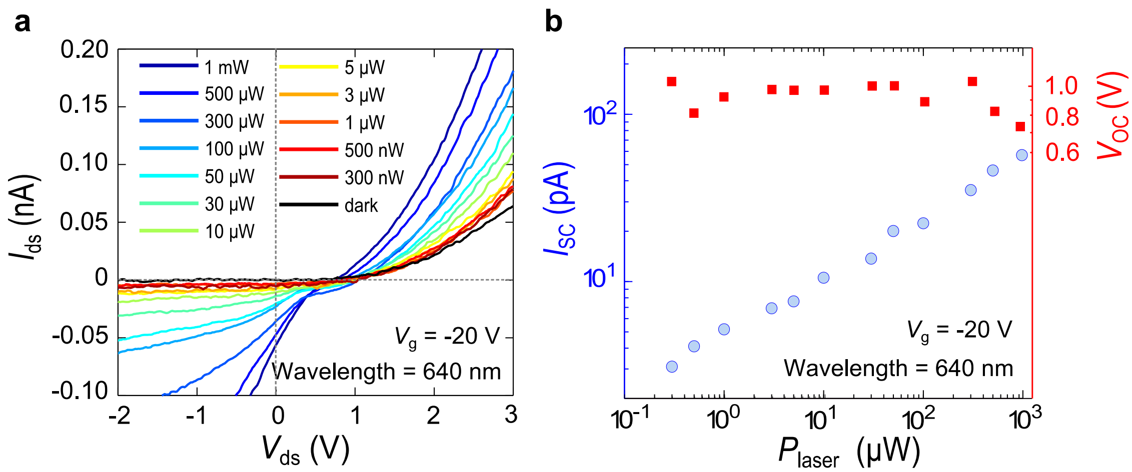


**Fig. S9** Power dependence on the photovoltaic effect of a CuPc-$MoS_2$ monolayer-based device. (a) $I_{ds}$-$V_{ds}$ curves measured at different optical powers and at fixed $V_g$ = -20 V and λ = 640 nm. (b) $I_{SC}$ and $V_{OC}$ values extracted from (a). A fairly constant $V_{OC}$ is obtained at all $P_{laser}$ values and $I_{SC}$ increasing with $P_{laser}$ following a power law.

The responsivity of the monolayer-$MoS_2$-based CuPc-$MoS_2$ device is tested for different incident optical powers and for $V_{ds}$ = -6 V, $V_g$ = -20 V and $\lambda$ = 640 nm. Similar values to the ones obtained for the bilayer-based device had been found, with computed EQE~10% at small incident optical powers.

**S8. Wavelength dependence of the photovoltaic effect in the CuPc-$MoS_2$ devices**

The $I_{sc}$ current generated in our CuPc-$MoS_2$ devices as a function of the wavelength (Fig 4d) resembles the light absorbance spectra of CuPc rather than that of $MoS_2$ (see References S3 and S4 for instance). The absorbance of CuPc has a minimum at a wavelength of 450 nm and monotonically increases up to a maximum at ~625 nm. It has a secondary maximum at ~700 nm. For larger frequencies the absorbance is reduced and is almost negligible for wavelengths larger than 850 nm. The correlation between the responsivity and the absorbance of CuPc suggest that the photocurrent in the CuPc-$MoS_2$ junction is mainly originated in the organic layer, which is in agreement with all other features observed (see main text).

## References


(S1) A. Ortiz-Conde, F. J. García Sánchez and J. Muci, *Solid-State electronics,* 2000, **44**, 1861-64.

(S2) M. M. Furchi, A. Pospischil, F. Libisch, J. Burgdörfer and T. Mueller, *Nano Lett*ers, 2014, **14**, 4785-4791.

(S3) Q. Li, J. Yu, Y. Zhang, N. Wang and Y. Jiang, *Front. Energy*, 2012, **6**, 179–183.

(S4) A. Splendiani, L. Sun, Y. Zhang, T. Li, J. Kim, C.-Y. Chim, G. Galli, F. Wang, *Nano Lett.* 2010, ***10***, 1271.